Nanoscale Research Letters

NANO EXPRESS Open Access

Nanoscale Effect of Zirconia Filler Surface on Mechanical Tensile Strength of Polymer Composites

Kai Kan[1,2,3], Daiki Moritoh[1], Yuri Matsumoto[1], Kanami Masuda[1], Masataka Ohtani[1,2,3*] and Kazuya Kobiro[1,2,3*]

Abstract

A characteristic effect of a nano-concave-convex structure of a zirconia nanoparticle assembly with an inherent porous structure and huge surface area enabled us to introduce systematic surface modification by thermal treatment to smooth surface and polymer impregnation to mask the nano-concave-convex structure of the zirconia nanoparticle assembly. A polymer composite prepared from 30 wt% poly(*N*-isopropylacrylamide) containing 0.02 wt% zirconia nanoparticle assembly with the inherent nano-concave-convex surface structure showed the highest tensile strength in mechanical tensile testing. However, both sintered zirconia nanoparticle assembly with smooth surface and zirconia nanoparticle assemblies with polymer masked surface showed lower strength with longer elongation at break in mechanical tensile testing.

Keywords: Nanoparticle, Nano-concave-convex, Impregnation, Surface modification, Polymer composite

Introduction

Nanomaterials are some of the most intriguing advanced materials in many research and application fields [1–5], since their intrinsic physical/chemical properties are so different from those of bulk materials [6–9]. When nanomaterials are applied as fillers of polymer composites, minute differences in the fillers, such as surface area, surface structure, and particle morphology of the nanomaterials, lead to drastic changes in the macro-scale properties of the composites [10].

For instance, incorporation of inorganic components into polymers improved physical and chemical properties, such as thermal stability, mechanical strength, dispersibility, and solubility [11–14].

However, a systematic study failed to clarify the relationship between the nanoscale properties of the nanomaterials, i.e., structure, morphology, and surface area, and the macro-scale physical and mechanical ones of the composites.

Porous metal oxide nanomaterials such as silicon dioxide [15–17], titanium dioxide [18–20], zirconium dioxide [21–23], cerium dioxide [24–26], and other materials [27–29] with large surface areas have been applied in chemical catalysis, gas absorption, separation, drug delivery, and energy storage materials [30–35]. In this context, our group developed unique metal oxide nanoparticle assemblies with submicron-sized spherical morphologies by a simple one-pot and single-step solvothermal approach [36]. We named these materials *m*icro/*m*esoporously *a*rchitected *r*oundly *i*ntegrated *m*etal *o*xides (MARIMOs). These produce nanometer-scale surface roughness and wide surface area. For instance, TiO_2 MARIMO has a nano-concave-convex surface due to its inherent numerous fine primary particles with diameters of ca. 5 nm and high specific surface area (400 m^2 g^{-1}) [35]. In previous research, we applied these unique materials to support inhomogeneous nanometal catalysts and anode materials for rechargeable batteries. In the catalyst supports, highly dispersed Au nanoparticles on the TiO_2 MARIMO support surface

* Correspondence: ohtani.masataka@kochi-tech.ac.jp; kobiro.kazuya@kochi-tech.ac.jp
[1]School of Environmental Science and Engineering, Kochi University of Technology, 185 Miyanokuchi, Tosayamada, Kochi 782-8502, Japan
Full list of author information is available at the end of the article

enhanced the catalytic activity and improved the durability of the catalyst at high temperature [37]. In the anode material, Nb_2O_5-TiO_2 MARIMO increased the current capacity and lifetime of the batteries [38]. Additionally, TiO_2 nanofiber bundles with a cheek brush morphology enhanced the mechanical strength of a polymer hydrogel when used as a filler [39].

The nano- and micro-scale anchoring effect is most significant in the adhesive mechanism. We consider that these MARIMOs with nano-concave-convex surface structures, huge surface areas, and porous structures would be appropriate for clarifying the relationship between nanoscale surface properties and macro-scale material properties, since the surface properties of MARIMO can be easily tuned by thermal treatment and polymer decoration (Fig. 1). For instance, thermal treatment of MARIMO creates a smooth surface with a decreased surface area and lower porosity. Impregnation [40] of monomers or polymers into MARIMO pores should mask the nano-concave-convex surface of the MARIMO. Thus, in this paper, a new method of filler surface modification by impregnation of polymers to mask the nano-concave-convex shape of MARIMO was studied to demonstrate the nano-anchoring effect of the filler surface. Here, we selected a zirconia (ZrO_2) MARIMO as a filler to enhance the mechanical properties of polymer composites, since ZrO_2 filler exhibits better properties such as chemical resistance especially for acids, mechanical strength, and thermal stability, which would be favorable for the polymeric matrix to lead durable polymer composites [41–43]. Monomers, 2-hydroxyethyl methacrylate (HEMA), benzyl methacrylate (BMA), and cyclohexyl methacrylate

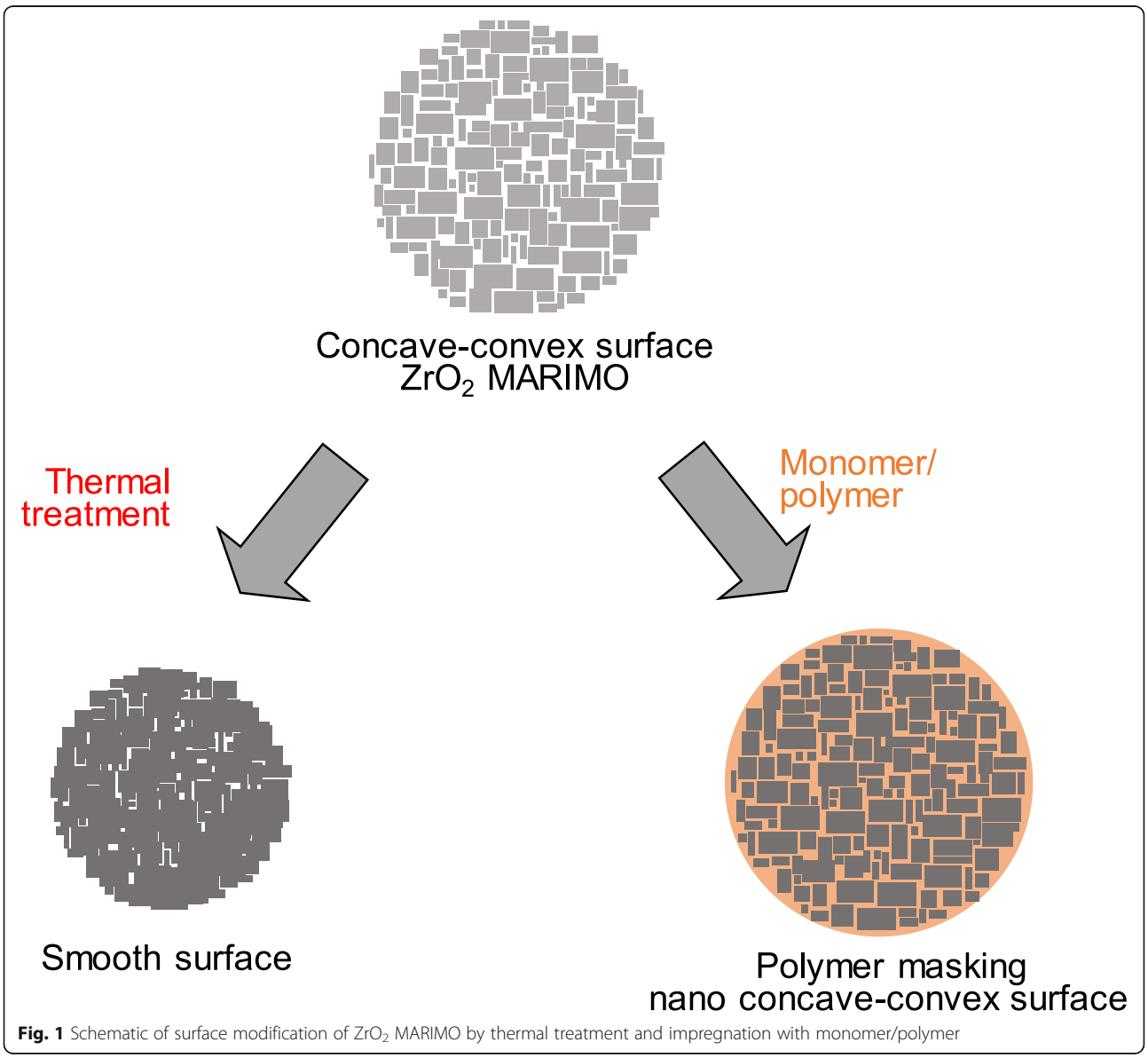

Fig. 1 Schematic of surface modification of ZrO_2 MARIMO by thermal treatment and impregnation with monomer/polymer

(CHMA), and their polymers were selected to modify the nano-concave-convex surface of ZrO_2 MARIMO fillers. Poly(*N*-isopropylacrylamide) (PNIPAM) hydrogel was chosen as a matrix for the polymer composites.

There are several approaches to estimate physical and chemical interactions between filler surfaces and polymer chains in polymer composites. Thermogravimetry, UV–visible spectroscopy, FT-IR spectroscopy, and microscopy are their representatives. Here, we adopted mechanical tensile testing as an alternative technique that is relatively simple, easy, and rapid. There are a few reports on mechanical property of the hydrogels with graphene oxide and ZrO_2 powder [44, 45], which is different from ours with respect to a simple system which consisted of only zirconia and polymer matrix. To the best of our knowledge, no report on the relationship between nanostructural changes in filler surfaces and polymer chains in polymer composites has been published.

Methods

Materials

N-isopropylacrylamide (NIPAM), *N,N,N′,N′*-tetramethylethylenediamine (TMEDA), potassium persulfate (KPS), and commercial zirconia (commercial ZrO_2) were purchased from FUJIFILM Wako Pure Chemical Corporation. HEMA, BMA, CHMA, and 1-hydroxycyclohexyl phenyl ketone (HCPK) were purchased from Tokyo Chemical Industry Co., Ltd. All reagents were used as received. ZrO_2 MARIMO was obtained from UJIDEN Chemical Industry Co., Ltd.

Preparation of HEMA-, NIPAM-, BMA-, and CHMA-Impregnated ZrO_2 MARIMO Fillers

An impregnation method for supported nanometal catalyst preparation [40] was applied to obtain HEMA-impregnated ZrO_2 MARIMO filler. ZrO_2 MARIMO was dried at 80 °C under vacuum for 12 h. Then, 20 μL of a HEMA/HCPK (20/1, mol/mol) mixture was added to 200 mg of vacuum-dried ZrO_2 MARIMO, and the mixture was manually mixed well with a mortar and pestle. It was then irradiated with UV light for 1 h with intermittent mixing every 15 min. Similar procedures were used to prepare NIPAM-, BMA-, and CHMA-impregnated ZrO_2 MARIMO fillers.

Preparation of PNIPAM Hydrogels with ZrO_2 Fillers

Hydrogels consisting of PNIPAM and ZrO_2 fillers were prepared according to a previously reported method [37]. ZrO_2 MARIMO (24 mg, 0.02 wt%) was dispersed in 115 mL of reverse osmosis water with N_2 bubbling before adding NIPAM (36 g, 30 wt%) to the solution. The mixture was stirred for 30 min and then KPS (0.18 g, 0.67 mmol) in water (5 mL) and TMEDA (1.8 mL, 12 mmol) were successively added. The mixture was carefully transferred to several glass tubes with an inner diameter of 1.0 cm. The upper dead volume of the tubes was purged with N_2 and the glass tubes were closed tightly with screw caps then left at 25 °C. After 3 days, the glass tubes were cut and the polymer hydrogels were removed. The obtained hydrogel rods with a diameter of 1.0 cm and length of 3.0 cm were used for mechanical strength measurements. Similar procedures afforded PNIPAM composites with HEMA-, NIPAM-, BMA-, and CHMA-impregnated ZrO_2 MARIMO fillers.

Mechanical Tensile Testing of Polymer Composites

Mechanical tensile testing was applied to the specimens in the axial direction. The deformed length of the composite (strain) and the applied force (stress) were measured using a tensile tester (AND MCT-2150) with a crosshead speed of 50 mm min^{-1} at room temperature. On the tensile tests of all composite samples, the percent elongation, 930%, is the limitation of the tensile tester machine. Ten composite samples were used for the mechanical tensile testing, and at least seven samples were used for data analysis. We note that composites containing bubble, cracked by glass, and cracked by grip of tensile testing machine were omitted from the data analysis to guarantee the data quality. The results are presented as mean ± standard deviation.

Characterization Methods

Scanning electron microscopy (SEM) was performed on a Hitachi SU8020 FE-SEM microscope. Transmission electron microscopy (TEM) images were obtained with a JEOL JEM-2100F microscope. STEM-EDX mapping was taken by bright-field (BF) mode and performed on an Oxford INCA X-max 80 EDX spectrometer. X-ray diffractometry (XRD) was performed on a Rigaku SmartLab diffractometer (Cu Kα radiation, D/teX Ultra 250 detector). Nitrogen adsorption–desorption isotherms were obtained using a BEL Japan Inc. Belsorp Mini (II) instrument. Specific surface areas were calculated using the Brunauer–Emmett–Teller (BET) method, and pore size distribution was derived by the Barrett–Joyner–Halenda (BJH) method. Differential scanning calorimetry (DSC) was performed with DSC7000X from Hitachi High-Tech Science Corporation at a scanning rate of 10 °C min^{-1} from 0 to 100 °C in a nitrogen atmosphere in three scans. Size exclusion chromatography (SEC) was performed using a JASCO PU-2080 Plus pump with two gel columns (KF-804L and KF-806L) and an RI-2031 Plus Intelligent RI detector in chloroform calibrated with polystyrene standards at 40 °C. Diffuse reflectance infrared Fourier transform spectroscopy (DRIFTS) was performed on a FT/IR-4600 from JASCO Corporation, and the spectra were performing Kubelka-Munk transformations.

Results and Discussion

Surface Properties of ZrO_2 MARIMOs

Physical properties of ZrO_2 fillers were evaluated by the BET method, XRD, and SEM. A reference material, commercial ZrO_2 nanoparticles, showed roughly aggregated morphology (Fig. 2a,b) with a specific surface area of 20 m^2 g^{-1} (Table 1). Conversely, ZrO_2 MARIMO exhibited a spherical mesoporous morphology (Fig. 2c,d) with a huge specific surface area (283 m^2 g^{-1}), which is 14 times larger than that of the commercial ZrO_2 nanoparticles. Sintered ZrO_2 MARIMO obtained by heating at 700 °C for 3 h in air exhibited a low specific surface area of 6 m^2 g^{-1} as expected (Fig. 2e,f). The extreme reduction in the specific surface area indicates that the primary particle size of the sintered ZrO_2 MARIMO was increased by heating, which was confirmed by primary

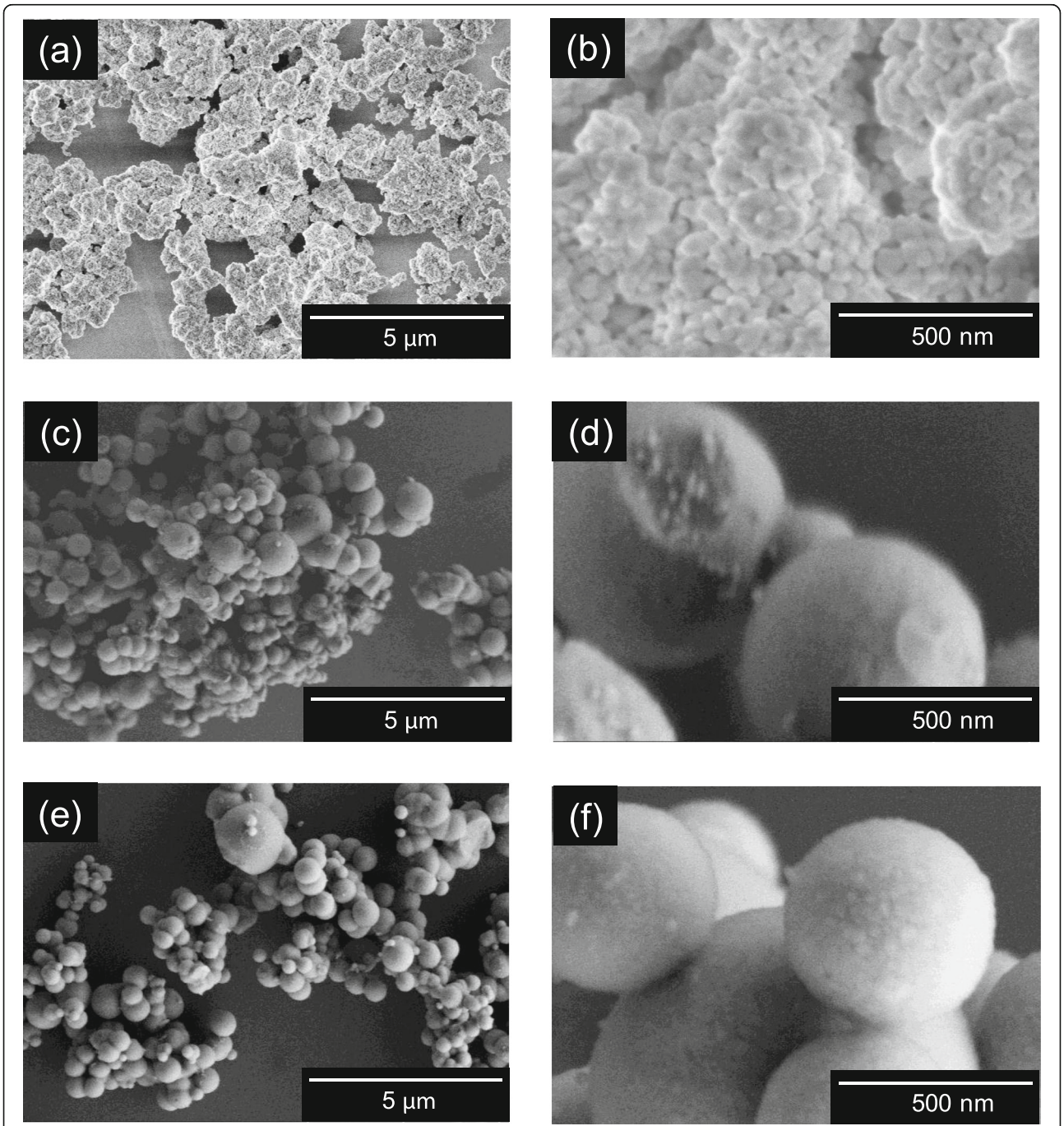

Fig. 2 SEM images of **a** low magnification and **b** high magnification of commercially available ZrO_2, **c** low magnification and **d** high magnification of ZrO_2 MARIMO, and **e** low magnification and **f** high magnification of sintered ZrO_2 MARIMO

Table 1 Specific surface area and primary particle size of ZrO_2 fillers

Filler	Specific surface are[a] (m^2 g^{-1})	Pore size[b] (nm)	Primary particle size[c] (nm)
Commercial ZrO_2	20	33	31
ZrO_2 MARIMO	283	2	1
Sintered ZrO_2 MARIMO	6	10	20

[a]Determined by BET method
[b]Determined by BJH method
[c]Estimated by the Scherrer equation

particle size estimation from the XRD peak width using the Scherrer equation and BJH method from the nitrogen adsorption–desorption isotherm analysis (Table 1). Thus, tiny primary particles in the ZrO_2 MARIMO brought huge surface area as well as porous structure with the nano-concave-convex surface. Therefore, much amount of materials will interact with the nano-concave-convex surface and pores of the ZrO_2 MARIMO.

DSC is a powerful tool to demonstrate the interaction between ZrO_2 filler surface and organic molecules through endo- or exo-thermal phenomena [45]. Prior to surface decollation of ZrO_2 MARIMO fillers by polymers, we selected NIPAM monomer as probe molecules to investigate the interaction between the ZrO_2 filler surface and organic probe molecules by means of DSC, since melting point of NIPAM monomer is sensitive to the crystallinity of NIPAM solid [46]. If NIPAM solid is embedded in pores of host materials, its melting point would shift to lower temperature, since the crystallinity of the embedded nano-sized NIPAM solid with nano-size in the pores of the host materials would be easily disturbed by some perturbation from boundary pore wall.

The DSC profiles of NIPAM itself, a mixture of commercial ZrO_2 nanoparticles and NIPAM monomer (commercial ZrO_2/NIPAM), a mixture of ZrO_2 MARIMO and NIPAM monomer (ZrO_2 MARIMO/NIPAM), and a mixture of sintered ZrO_2 MARIMO and NIPAM monomer (sintered ZrO_2 MARIMO/NIPAM) with different ZrO_2/NIPAM ratio in weight are shown in Fig. S1, Fig. S2, and Fig. S3, respectively. NIPAM monomer itself showed an endothermal peak ascribed to its melting point at 67.7 °C. In the case of commercial ZrO_2/NIPAM, a simple gradual peak shift of DSC profiles from 67.7 °C (NIPAM) to 64.8 °C was observed in accordance with the higher ZrO_2 contents (Fig. S1, Table S1). The endothermal peaks at 64.8 °C can be ascribed to the melting point of NIPAM solid situated between the commercial ZrO_2 primary particles.

On the contrary, the larger temperature shifts from 67.7 to 62.4 °C were recognized in accordance with the higher ZrO_2 MARIMO contents up to ZrO_2 MARIMO/NIPAM = 50/50 (wt%) in the case of ZrO_2 MARIMO/NIPAM (Fig. S2, Table S1). These large shifts clearly demonstrate that the ZrO_2 MARIMO has some positive effect on solid state of NIPAM monomer embedded in the MARIMO pores, where the larger shift of the endothermal peaks could correspond to the stronger interaction between the ZrO_2 filler surface and NIPAM monomer. However, the endothermal peaks were shifted to opposite direction of higher temperature of 65.2 °C at the ZrO_2/NIPAM ratio ranging from 50/50 to 80/20 (wt%). It is difficult to put forward a conclusive discussion, but the endothermal peaks at 62.4 and 65.2 °C might be ascribed to the melting points of NIPAM solid embedded deep pores and much amount of shallow pores in ZrO_2 MARIMO, respectively. As for the sintered ZrO_2 MARIMO/NIPAM with the smooth surface, quite similar simple lower temperature shifts of endothermal peaks were shown in proportion to sintered ZrO_2 MARIMO contents (Fig. S3, Table S1) similar to the results of commercial ZrO_2/NIPAM in Fig. S1.

Thus, the positive interaction found between the ZrO_2 MARIMO and NIPAM monomer would be advantageous to polymer decollation onto the ZrO_2 MARIMO surface.

Preparation of PNIPAM Hydrogels with ZrO_2 Fillers

To evaluate the effect of surface structure of the ZrO_2 fillers further, PNIPAM hydrogels with the ZrO_2 fillers were chosen, since strength of PNIPAM hydrogels were sensitive to the properties of the fillers. PNIPAM hydrogels were prepared from aqueous solutions containing different amounts (20, 25, and 30 wt%) of NIPAM, KPS as a radical initiator, and TMEDA. When the gel obtained from 20 wt% of NIPAM was left at room temperature, it changed to sol within 60 min (Fig. S4a). Conversely, no structural deformation of the hydrogel shape was observed with the gels obtained from 25 and 30 wt% NIPAM solutions (Fig. S4b–c). The stress and strain were 2.7 ± 0.2 kPa and above 930% for 25 wt% PNIPAM hydrogels, and 7.8 ± 0.2 kPa and 716 ± 106% for 30 wt% PNIPAM hydrogels, respectively (Fig. S5 and Table S2). Then, we selected the stronger 30 wt% PNIPAM hydrogel as a polymer matrix to evaluate the effect of the ZrO_2 fillers.

The ZrO_2 filler content in PNIPAM hydrogels was then optimized by changing the amount of the commercial ZrO_2 filler (0.002 (2a), 0.02 (2b), and 0.04 wt% (2c)) in 30 wt% of PNIPAM hydrogel. Consequently, composite 2a showed the highest tensile strength (9.5 ± 0.7 kPa), while composite 2b showed the highest elongation (902 ± 28%) among all composites (Fig. S6 and Table S3). From these results, it is difficult to judge which one (high tensile strength or long elongation) is suitable for the filler amount to prepare polymer hydrogel. Then, the profile areas were calculated to estimate how much work was necessary to break these composites. Consequently, composite 2b showed the highest work among all the composites (Table S3).

Thus, the conditions of 30 wt% of NIPAM and 0.02 wt% of ZrO_2 filler were fixed throughout the experiments.

Mechanical Tensile Testings of the Polymer Composites

The mechanical tensile strength obtained from stress–strain curves is shown in Fig. 3. The maximum stress and strain of each composite estimated from mechanical tensile testings are summarized in Table 2. The effect of the surface morphology of ZrO_2 filler on polymer composites can be clarified by measuring the tensile strength [41–43] of composites prepared with commercial ZrO_2 (2b), with nano-concave-convex ZrO_2 MARIMO (3), with and sintered ZrO_2 MARIMO (4) with the smooth surface. As a result, composite 3 containing MARIMO with the nano-concave-convex surface showed the highest ultimate tensile strength (9.2 ± 0.2 kPa) and the lowest elongation (746 ± 37%). However, composite 4 containing sintered MARIMO with a smooth surface exhibited a poor tensile strength of 6.6 ± 0.3 kPa. Elongation capacities of 2b (902 ± 28%) and 4 (903 ± 19%) were almost the same. Generally, the anchor effect of filler surface on polymer chains and slippage of polymer chains can be estimated from the maximum stress and maximum strain, respectively, obtained from mechanical tensile testing [47]. The obtained results clearly indicate that the nano-concave-convex surface played a critical role in the tensile strength of the polymer composites as expected, which can be an anchoring effect between the nano-concave-convex surface and the polymer chains in the polymer composites. In order to know the microstructure and distribution of ZrO_2 fillers, we used freeze-dried polymer composites for direct SEM observation. As a result, we confirmed the uniform polymer network of hydrogel but no aggregation nor agglomeration of ZrO_2 fillers was observed (Fig. S7).

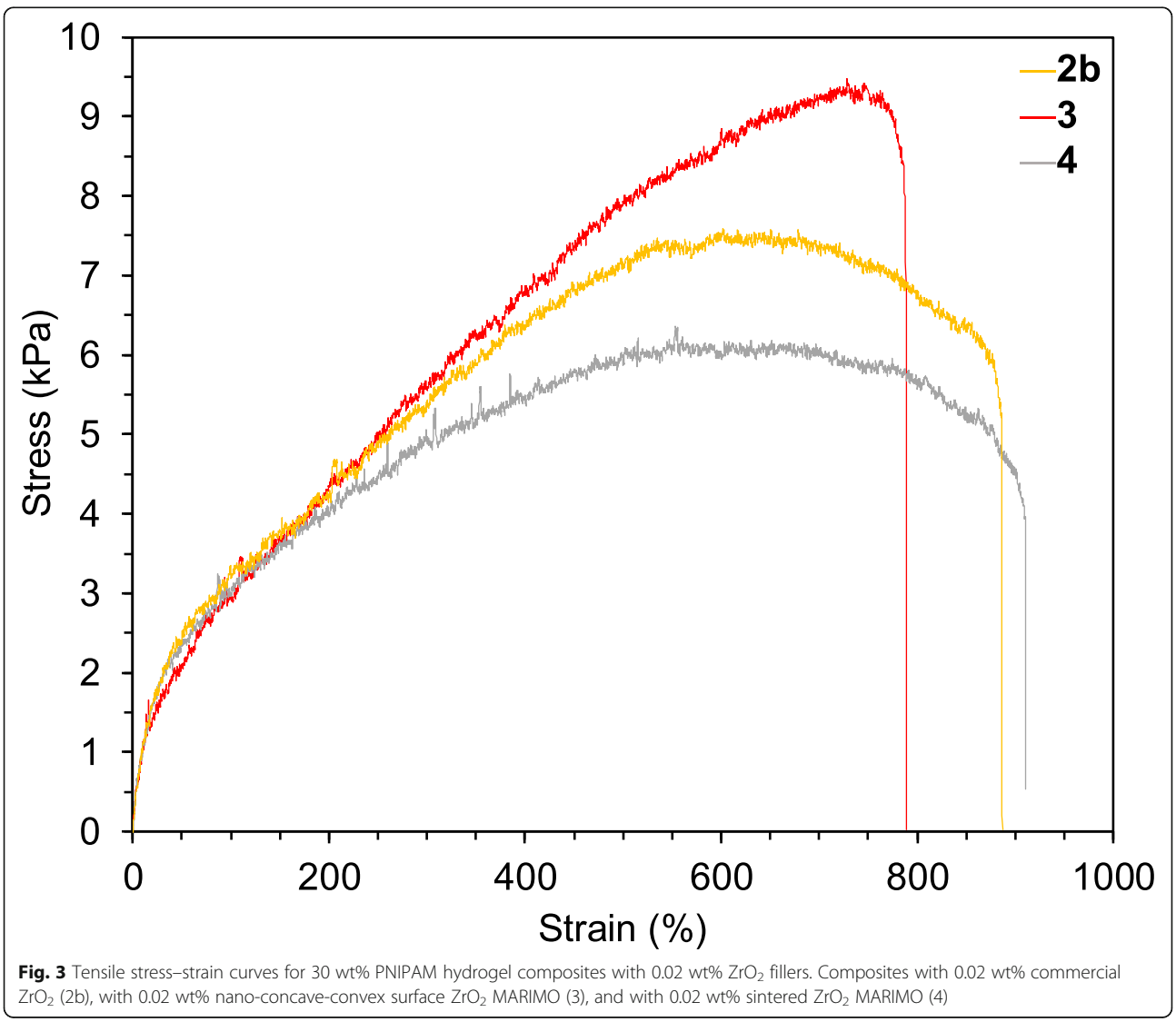

Fig. 3 Tensile stress–strain curves for 30 wt% PNIPAM hydrogel composites with 0.02 wt% ZrO_2 fillers. Composites with 0.02 wt% commercial ZrO_2 (2b), with 0.02 wt% nano-concave-convex surface ZrO_2 MARIMO (3), and with 0.02 wt% sintered ZrO_2 MARIMO (4)

Table 2 Tensile strengths and elongation capacities of 30 wt% PNIPAM hydrogel composites with 0.02 wt% ZrO_2 nano assembly

Composite	Filler	$Stress_{MAX}$ (kPa)	$Strain_{MAX}$ (%)
1	–	7.8 ± 0.2	716 ± 106
2b	Commercial ZrO_2	7.7 ± 0.2	902 ± 28
3	ZrO_2 MARIMO	9.2 ± 0.2	746 ± 37
4	Sintered ZrO_2 MARIMO	6.6 ± 0.3	903 ± 19

Effect of Surface Properties of Polymer-Impregnated ZrO_2 MARIMO

To complete the systematic study on the relationship between the nano-concave-convex surface of the ZrO_2 MARIMO filler and polymer chains, we modified the ZrO_2 MARIMO filler surface by polymer impregnation to mask the nano-concave-convex surface. Herein, we selected vinyl monomers such as HEMA, NIPAM, BMA, and CHMA to be impregnated into pores of ZrO_2 MARIMO. Polymerization of the impregnated monomers in ZrO_2 MARIMO was achieved by UV irradiation in the presence of a photoinitiator (HCPK). The progress of polymerization was checked by SEC of the supernatant of the impregnated ZrO_2 MARIMO/chloroform dispersion (Table S4). All the samples had molecular weights of around 1000. On DRIFTS experiments, there is no significant peak indicating interaction between the polymer and ZrO_2 MARIMO (Fig. S8). In this meaning, we studied SEM and STEM-EDX analysis to confirm impregnation. As shown in Fig. 4, the spherical MARIMO morphologies were retained even after the impregnation treatments. STEM-EDX analysis (Fig. 5) clearly shows that Zr, C, O, and (N) atoms were homogeneously distributed throughout the ZrO_2 MARIMO fillers. These results indicate that the monomers were uniformly impregnated and polymerized in the nanocavities and pores of the MARIMO.

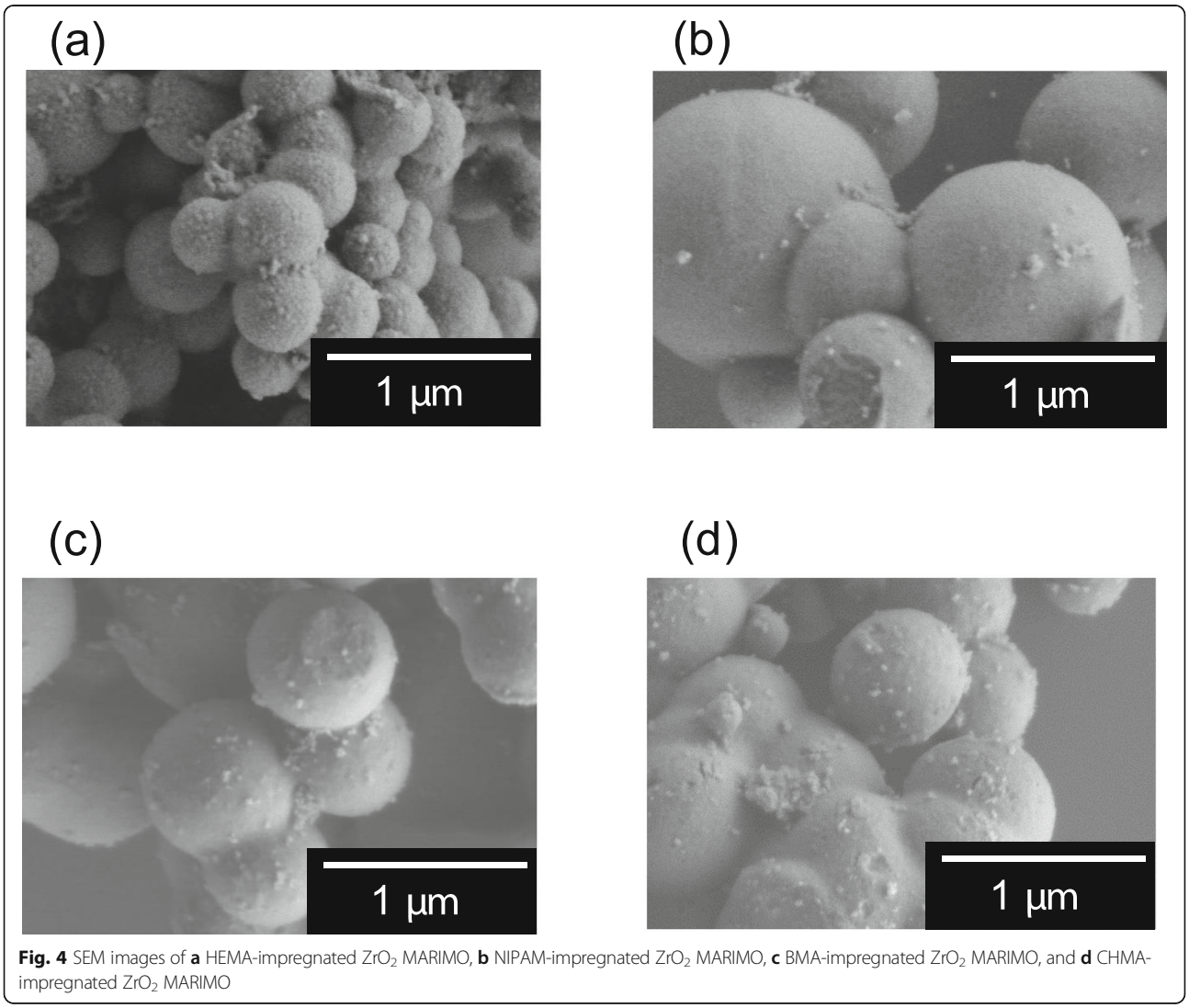

Fig. 4 SEM images of **a** HEMA-impregnated ZrO_2 MARIMO, **b** NIPAM-impregnated ZrO_2 MARIMO, **c** BMA-impregnated ZrO_2 MARIMO, and **d** CHMA-impregnated ZrO_2 MARIMO

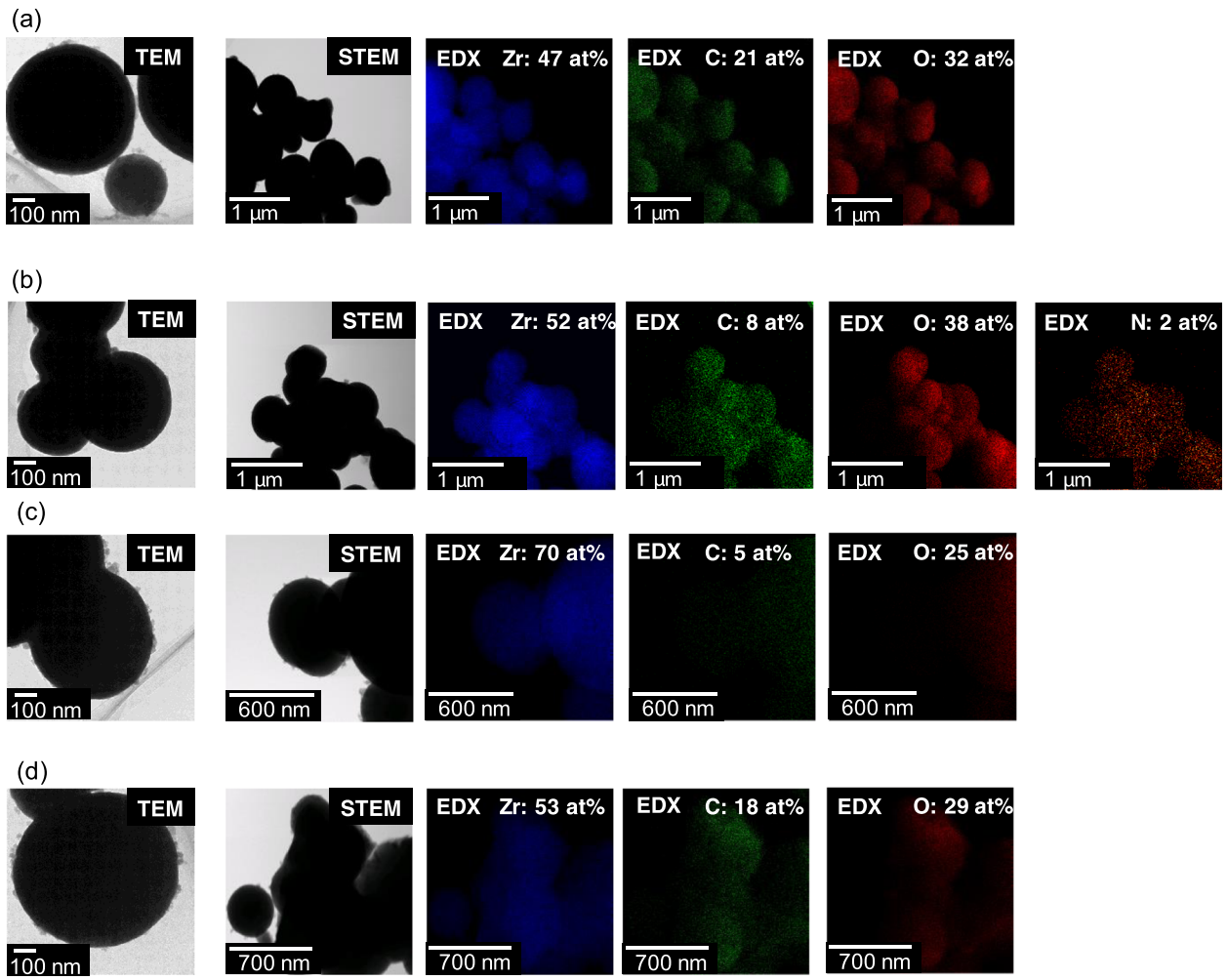

Fig. 5 TEM and STEM-EDX mapping images of **a** HEMA-impregnated ZrO_2 MARIMO, **b** NIPAM-impregnated ZrO_2 MARIMO, **c** BMA-impregnated ZrO_2 MARIMO, and **d** CHMA-impregnated ZrO_2 MARIMO

Mechanical Tensile Testings of Polymer Composites

Existence of the anchoring effect of the nano-concave-convex surface of ZrO_2 MARIMO was studied through mechanical tensile testings. Polymer composites with HEMA-impregnated ZrO_2 MARIMO (5), with NIPAM-impregnated ZrO_2 MARIMO (6), with BMA-impregnated ZrO_2 MARIMO (7), and with CHMA-impregnated ZrO_2 MARIMO (8) were prepared according to the similar procedures to that employed for composites 2b, 3, and 4. As shown by the mechanical tensile strengths obtained from stress–strain curves in Fig. 6, all composites 5–8 with vinyl polymer impregnated ZrO_2 MARIMO fillers showed lower tensile strength as compared to composite 3 with the nano-concave-convex ZrO_2 MARIMO filler (Table 3), suggesting the anchoring effect of the surface reduced in all cases of the polymer impregnated ZrO_2 MARIMO fillers. Instead, higher elongation of all composites 5–8 with the polymer impregnated ZrO_2 MARIMO fillers was clearly observed, which can be ascribed to slippage of the matrix polymer chains on the polymer-impregnated MARIMO filler surfaces. Thus, polymer-impregnated ZrO_2 MARIMO fillers in polymer composites induced lower tensile strength and improved elongation capacity of the composites. Turning to the protopype ZrO_2 MARIMO, the nano-concave-convex surface played a positive role in the tensile strength of the polymer composites.

Conclusion

Surface modification of a ZrO_2 MARIMO filler with a nano-concave-convex structure revealed importance of nanoscale anchoring interactions between the filler surface and matrix polymer chains via mechanical tensile testings. To investigate the effect of the nano-concave-convex structure, we modified the ZrO_2 MARIMO filler surface by (i) calcination of the ZrO_2 MARIMO to smooth the nano-concave-convex surface and (ii) impregnation of polymers into the ZrO_2 MARIMO pores

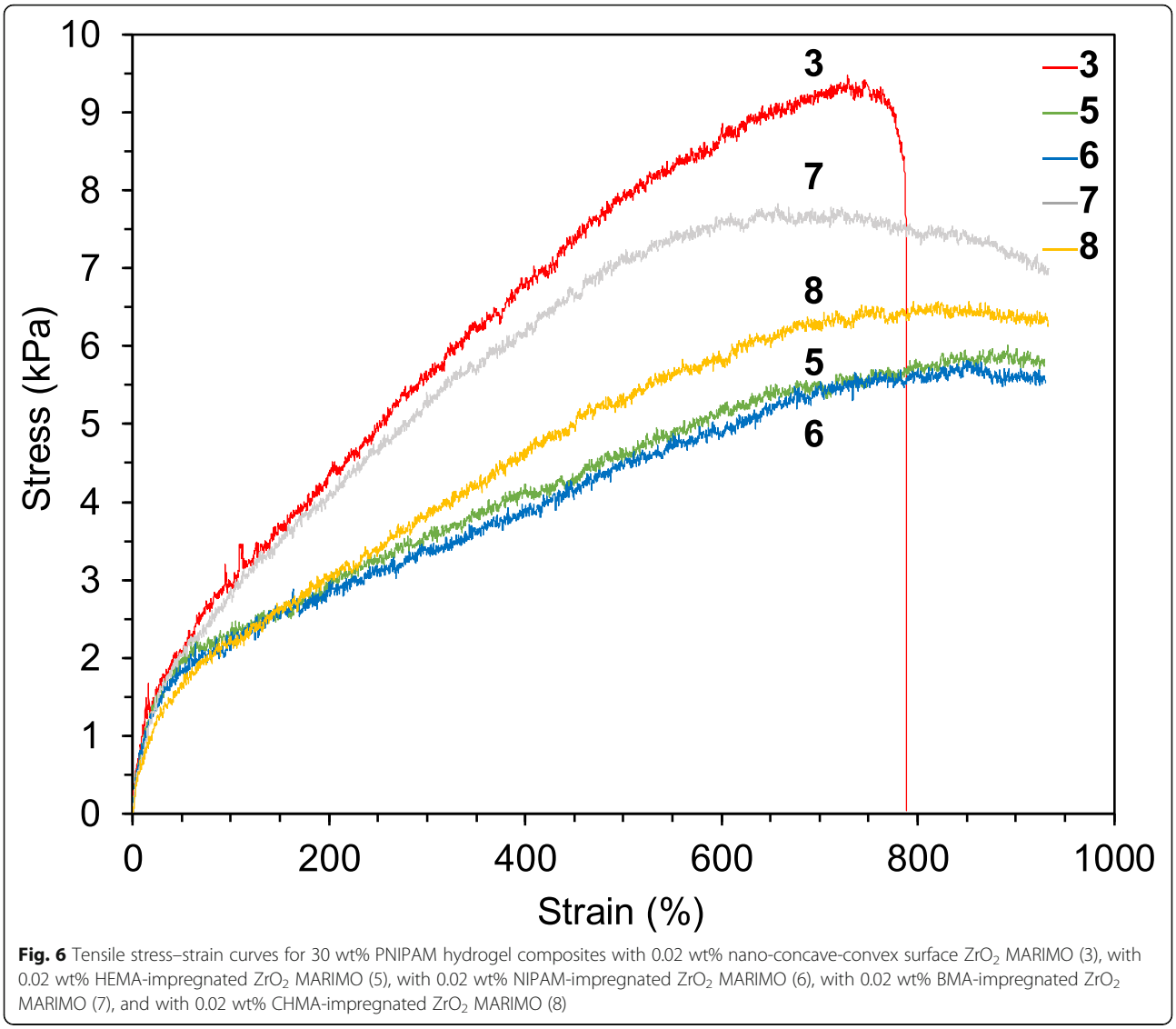

Fig. 6 Tensile stress–strain curves for 30 wt% PNIPAM hydrogel composites with 0.02 wt% nano-concave-convex surface ZrO_2 MARIMO (3), with 0.02 wt% HEMA-impregnated ZrO_2 MARIMO (5), with 0.02 wt% NIPAM-impregnated ZrO_2 MARIMO (6), with 0.02 wt% BMA-impregnated ZrO_2 MARIMO (7), and with 0.02 wt% CHMA-impregnated ZrO_2 MARIMO (8)

to mask the nano-concave-convex surface. Mechanical tensile testing was applied to estimate the interaction between the surface of the fillers and the polymer chains in the polymer composites. The polymer composites containing a nano-concave-convex ZrO_2 MARIMO filler showed the highest tensile strength, while polymer-impregnating the ZrO_2 MARIMO fillers caused the large elongation. Thus, the nano-concave-convex surface of the ZrO_2 MARIMO filler positively interacted with the matrix polymer chains to improve the tensile strength capacity, while polymer-masking the nano-concave-convex surface of the ZrO_2 MARIMO fillers improved the elongation capacity. Consequently, rational design of the filler surface enabled us to understand the nanoscale

Table 3 Tensile strengths and elongation capacities of 30 wt% PNIPAM hydrogel composites with 0.02 wt% polymer-impregnated ZrO_2 MARIMOs

Composite	Filler	$Stress_{MAX}$ (kPa)	$Strain_{MAX}$ (%)
5	HEMA-impregnated ZrO_2 MARIMO	6.1 ± 0.2	> 930[a]
6	NIPAM-impregnated ZrO_2 MARIMO	5.9 ± 0.3	> 930[a]
7	BMA-impregnated ZrO_2 MARIMO	7.9 ± 0.3	> 930[a]
8	CHCA-impregnated ZrO_2 MARIMO	6.7 ± 0.2	> 930[a]

[a]The percent elongation more than 930% means the limitation of tensile tester machine

interaction of filler surface with the polymer matrix through macro-scale mechanical tensile testings. Different kinds of monomers or polymers, such as ionic, hydrophilic, and hydrophobic monomers or polymers, can be incorporated into the MARIMO fillers by the simple impregnation technique to control properties of MARIMO fillers. Further studies on better dispersion of ZrO_2 filler into aqueous media is now in progress.

Supplementary information

Supplementary information accompanies this paper at https://doi.org/10.1186/s11671-020-3282-6.

Additional file 1. Supporting Information. Photographs of PNIPAM hydrogels, stress-strain curves and mechanical properties of polymer hydrogels, and SEC results of polymer impregnated ZrO_2 MARIMOs.

Abbreviations

BET: Brunauer–Emmett–Teller; BF: Bright-field; BJH: Barrett–Joyner–Halenda; BMA: Benzyl methacrylate; CHMA: Cyclohexyl methacrylate; DRIFTS: Diffuse reflectance infrared Fourier transform spectroscopy; DSC: Differential scanning calorimetry; HCPK: 1-Hydroxycyclohexyl phenyl ketone; HEMA: 2-Hydroxyethyl methacrylate; KPS: Potassium persulfate; MARIMO: Micro/mesoporously architected roundly integrated metal oxide; NIPAM: *N*-Isopropylacrylamide; PNIPAM: Poly(*N*-isopropylacrylamide); SEC: Size exclusion chromatography; SEM: Scanning electron microscopy; TEM: Transmission electron microscopy; TMEDA: *N,N,N′,N′*-tetramethylethylenediamine; XRD: X-ray diffractometry; ZrO_2: Zirconia

Acknowledgements

The authors also thank Ujiden Chemical Industry Co., Ltd. for providing them with ZrO_2 MARIMO.

Authors' Contributions

K. Kan contributed to the research planning, data analysis, and writing of manuscript. DM, YM, and KM contributed to the experiments. MO and K. Kobiro contributed to help in data analysis, discussion, and manuscript modification. All authors read and approved the final manuscript.

Funding

This work was supported by the financial support from the Creation of New Business and Industry Program through the Kochi Prefectural Industry Academia Government Collaboration Research Promotion Operation.

Availability of Data and Materials

All relevant data that support the findings of this study are available from the corresponding author on request.

Competing Interests

The authors declare that they have no competing interests.

Author details

[1]School of Environmental Science and Engineering, Kochi University of Technology, 185 Miyanokuchi, Tosayamada, Kochi 782-8502, Japan. [2]Laboratory for Structural Nanochemistry, Kochi University of Technology, 185 Miyanokuchi, Tosayamada, Kochi 782-8502, Japan. [3]Research Center for Material Science and Engineering, Kochi University of Technology, 185 Miyanokuchi, Tosayamada, Kochi 782-8502, Japan.

Received: 11 December 2019 Accepted: 17 February 2020
Published online: 02 March 2020

References

1. Zheng M, Jagota A, Semke ED, Diner BA, McLean RS, Lustig SR, Richardson RE, Tassi NG (2003) DNA-assisted dispersion and separation of carbon nanotubes. Nat Mater 2:338–342
2. Gates BD, Xu Q, Stewart M, Ryan D, Willson CG, Whitesides GM (2005) New approaches to nanofabrication: molding, printing, and other techniques. Chem Rev 105:1171–1196
3. Farokhzad OC, Langer R (2009) Impact of nanotechnology on drug delivery. ACS Nano 3:16–20
4. Qin D, Xia Y, Whitesides GM (2010) Soft lithography for micro- and nanoscale patterning. Nat Protoc 5:491–502
5. Liu M, Ishida Y, Ebina Y, Sasaki T, Hikima T, Takata M, Aida T (2015) An anisotropic hydrogel with electrostatic repulsion between cofacially aligned nanosheets. Nature 517:68–72
6. Valtchev V, Tosheva L (2013) Porous nanosized particles: preparation, properties, and applications. Chem Rev 113:6734–6760
7. Xu Y, Zhang B (2014) Recent advances in porous Pt-based nanostructures: synthesis and electrochemical applications. Chem Soc Rev 43:2439–2450
8. Zhu CZ, Du D, Eychmüller A, Lin YH (2015) Engineering ordered and nonordered porous noble metal nanostructures: synthesis, assembly, and their applications in electrochemistry. Chem Rev 115:8896–8943
9. Ohtani M, Muraoka T, Okimoto Y, Kobiro K (2017) One-pot solvothermal batch synthesis of porous nanocrystal assemblies composed of multiple transition metal elements. Inorg Chem 56:11546–11551
10. Sanchez C, Belleville P, Popall M, Nicole L (2011) Applications of advanced hybrid organic-inorganic nanomaterials: from laboratory to market. Chem Soc Rev 40:696–753
11. Xu L, Shyu TC, Kotov NA (2017) Origami and kirigami nanocomposites. ACS Nano 11:7587–7599
12. Wei J, Wang F, Zhang L (2018) Micropatterning of highly stretchable tough polymer actuators for multistage detection of acetone vapors. ACS Appl Mater Interfaces 10:29161–29168
13. Chen T, Hou K, Ren Q, Chen G, Wei P, Zhu M (2018) Nanoparticle–polymer synergies in nanocomposite hydrogels: from design to application. Macromol Rapid Commun 39:1800337
14. Zhao N, Yan L, Zhao X, Chen X, Li A, Zheng D, Zhou X, Dai X, Xu FJ (2019) Versatile types of organic/inorganic nanohybrids: from strategic design to biomedical applications. Chem Rev 119:1666–1762
15. Yang PP, Gai SL, Lin J (2012) Functionalized mesoporous silica materials for controlled drug delivery. Chem Soc Rev 41:3679–3698
16. Biju V (2014) Chemical modifications and bioconjugate reactions of nanomaterials for sensing, imaging, drug delivery and therapy. Chem Soc Rev 43:744–764
17. Ke FY, Yi JH, Zhang SQ, Ravikovitch PI, Kruk M (2019) Structures and dimensions of micelle-templated nanoporous silicas derived from swollen spherical micelles of temperature-dependent size. J Colloid Interface Sci 544:312–320
18. Wang XJ, Feng J, Zhang Q, Yin YD (2016) Synthesis, properties, and applications of hollow micro-/nanostructures. Chem Rev 116:10983–11060
19. Boyjoo Y, Wang MW, Pareek VK, Liu J, Jaroniec M (2016) Synthesis and applications of porous non-silica metal oxide submicrospheres. Chem Soc Rev 45:6013–6047
20. Low JX, Cheng B, Yu JG (2017) Surface modification and enhanced photocatalytic CO_2 reduction performance of TiO_2: a Review. Appl Surf Sci 392:658–686
21. Soo MT, Kawamura G, Muto H, Matsuda A, Lockman Z, Cheong KY (2013) Design of hierarchically meso-macroporous tetragonal ZrO_2 thin films with tunable thickness by spin-coating via Sol-Gel template route. Micropor Mesopor Mater 167:198–206
22. Sreethawong T, Ngamsinlapasathian S, Yoshikawa S (2013) Synthesis of crystalline mesoporous-assembled ZrO_2 nanoparticles via a facile surfactant-aided Sol-Gel process and their photocatalytic dye degradation activity. Chem Eng Sci 228:256–262
23. Wang C, Le Y, Cheng B (2014) Fabrication of porous ZrO_2 hollow sphere and its adsorption performance to Congo Red in water. Ceram Int 40:10847–10856
24. Zhao Y-X, Nie Z-W, Shi M-M, Zeng C-H, Wang L, Zhong S-L (2015) Cerium-based porous coordination polymers with hierarchical superstructures: fabrication, formation mechanism and their thermal conversion to hierarchical CeO_2. Inorg Chem Front 2:567–575
25. Latta P, Dhanabackialakshmi R, Kumar P, Karuthapandian S (2016) Synergistic effects of trouble free and 100% recoverable CeO_2/nylon nanocomposite thin film for the photo-catalytic degradation of organic contaminants. Sep Purif Technol 168:124–133
26. Wang ZM, Yu RB (2019) Hollow micro/nanostructured ceria based materials: synthetic strategies and versatile applications. Adv Mater 31:1800592

27. Li W, Liu J, Zhao D (2016) Mesoporous materials for energy conversion and storage devices. Nat Rev Mater 1:16023–16040
28. Benzigar MR, Talapaneni SN, Joseph S, Ramadass K, Singh G, Scaranto J, Ravon U, Al-Bahily K, Vinu A (2018) Recent advances in functionalized micro and mesoporous carbon materials: synthesis and applications. Chem Soc Rev 47:2680–2721
29. Zong LB, Wang ZM, Yu RB (2019) Lanthanide, doped photoluminescence hollow structures: recent advances and applications. Small 15:1804510
30. Samuel MS, Shah SS, Bhattacharya J, Subramaniam K, Singh NDP (2018) Adsorption of Pb (II) from aqueous solution using a magnetic chitosan/graphene oxide composite and its toxicity studies. Int J Biol Macromol 115: 1142–1150
31. Samuel MS, Subramaniyan V, Bhattacharya J, Parthiban C, Chand S, Singh NDP (2018) A GO-CS@MOF [Zn(BDC)(DMF)] material for the adsorption of chromium(VI) ions from aqueous solution. Compos Part B Eng 152:116–125
32. Samuel MS, Bhattacharya J, Parthiban C, Viswanathan G, Singh NDP (2018) Ultrasound-assisted synthesis of metal organic framework for the photocatalytic reduction of 4-nitrophenol under direct sunlight. Ultrason Sonochem 49:215–221
33. Samuel MS, Bhattacharya J, Raj S, Santhanam N, Singh H, Singh NDP (2019) Efficient removal of Chromium (VI) from aqueous solution using chitosan grafted graphene oxide (CS-GO) nanocomposite. Int J Biol Macromol 121:285–292
34. Samuel MS, Jose S, Selvarajan E, Mathimani T, Pugazhendhi A (2020) Biosynthesized silver nanoparticles using Bacillus amyloliquefaciens; Application for cytotoxicity effect on A549 cell line and photocatalytic degradation of p-nitrophenol. J Photochem Photobiol B Biol 202:111642
35. Wang P, Kobiro K (2014) Synthetic versatility of nanoparticles: a new, rapid, one-pot, single-step synthetic approach to spherical mesoporous (metal) oxide nanoparticles using supercritical alcohols. Pure Appl Chem 86:785–800
36. Wang P, Kobiro K (2012) Ultimately simple one-pot synthesis of spherical mesoporous TiO_2 nanoparticles in supercritical methanol. Chem Lett 41: 264–266
37. Duriyasart F, Irizawa A, Hayashi K, Ohtani M, Kobiro K (2018) Sintering-resistant metal catalysts supported on concave-convex surface of TiO_2 nanoparticle assemblies. ChemCatChem 10:3392–3396
38. Tanaka Y, Usui H, Domi Y, Ohtani M, Kobiro K, Sakaguchi H (2019) Mesoporous spherical aggregates consisted of Nb-doped anatase TiO_2 nanoparticles for Li and Na storage material. ACS Appl Energy Mater 2:636–643
39. Duriyasart F, Hamauzu H. Ohtani M, Kobiro K (2016), Three-dimensionally branched titanium dioxide with Cheek-Brush morphology: synthesis and its application to polymer composites. ChemistrySelect 1:5121–5128
40. Haruta M (2011) Spiers Memorial Lecture Role of perimeter interfaces in catalysis by gold nanoparticles. Faraday Discuss 152:11–32
41. Hu Y, Gu G, Zhou S, Wu L (2011) Preparation and properties of transparent PMMA/ZrO_2 nanocomposites using 2-hydroxyethyl methacrylate as a coupling agent. Polymer 52:122–129
42. Yu W, Wang X, Tang Q, Guo M, Zhao J (2014) Reinforcement of denture base PMMA with ZrO_2 nanotubes. J Mech Behav Biomed Mater 32:192–197
43. Gad MM, Fouda SM, Al-Harbi FA, Näpänkangas R, Raustia A (2017) PMMA denture base material enhancement: a review of fiber, filler, and nanofiller addition. Int J Nano-medicine 12:3801–3812
44. Hyang K, Wu H, Jiang F, Shen G, Wang L (2018) On the near-infrared light-responsive and mechanical properties of PNIPAM-based nanocomposite hydrogels. Polym Degrad Stabil 156:228–233
45. Michael FM, Krishnan MR, Fathima A, Busaleh A, Almohsin A, Alsharaeh EH (2019) Zirconia/graphene nanocomposites effect on the enhancement of thermo-mechanical stability of polymer hydrogels. Mater Today Commun 21:100701
46. Sasaki S, Okabe S (2010) Thermodynamic properties of N-isopropylacrylamide in water: solubility transition, phase separation of supersaturated solution, and glass formation. J Phys Chem B 114:14995–15002
47. Meijer HEH, Govaert LE (2005) Mechanical performance of polymer systems: the relation between structure and properties. Prog Polym Sci 30:915–938

Publisher's Note